Steam oxidation of chromium corrosion barrier coatings for SiC-based accident tolerant fuel cladding

K.A. Kane, P.I.M. Stack*, P.A. Mouche, R.R. Pillai, B.A. Pint

Materials Science and Technology Division, Oak Ridge National Laboratory, Oak Ridge, TN, US

*College of Engineering, University of Akron, Akron, OH, US

ABSTRACT

SiC-based materials are currently being considered for accident tolerant fuel (ATF) cladding, however, there are concerns regarding hydrothermal corrosion rates and hermeticity. These issues may be addressed with the utilization of a Cr corrosion barrier coating (CBC) but the interaction of Cr with SiC under loss of coolant accident (LOCA) conditions needs to be investigated. In the present work, Cr coatings were deposited onto chemically vapor deposited (CVD) SiC with either high power impulse magnetron sputtering (HiPIMS), cathodic arc (CA), or a combination of both. Annealing and steam thermogravimetric analysis (TGA) was used to study reaction product formation with and without oxidation. After 1200°C annealing, formation of a Cr_xC_y carbide layer at the ambient interface and a $Cr_xSi_yC_z$ silicide layer at the SiC interface was observed. After 1200°C TGA exposure, similar carbide and silicide layers were observed but with a Cr_2O_3 outer reaction layer and a Si and O rich interfacial layer forming between the carbide and silicide layers. Initial mass gain of the coatings during the 1200°C TGA exposure was parabolic and were similar to reported rates of chromia formation. Mass gain behavior and observed transitions in chromia microstructure indicate that metallic Cr may be consumed within the first ~1 h at 1200°C and that subsequent chromia formation occurs at the expense of the underlying Cr carbide layer. Overall, the results show no detrimental impact of Cr coatings on the steam oxidation resistance of SiC up to 4 h at 1200°C.

INTRODUCTION

Traditional Zr-based alloys have attractive properties for fuel cladding operation, but are extremely susceptible to high temperature steam oxidation during loss-of-coolant accidents (LOCA) in nuclear light water reactors (LWRs) [1]. Such an accident is marked by increasing core temperatures as H_2O flashes to steam [2], which can lead to cladding ballooning, loss of coolable geometry [3], cladding rupture, and potential fuel expulsion. Due to exceptional steam oxidation resistance [4,5] and high temperature strength [6,7], SiC_m/SiC_f ceramic matrix composites (CMCs) are being investigated as potential LWR accident tolerant fuel (ATF) cladding [8,9] and other core components [10].

A significant barrier to utilization of SiC/SiC CMCs as ATF cladding [8] is the feasibility of fully hermetic SiC/SiC CMCs [11–13]. Chromium coatings are a promising ATF concept [14] and can act as a corrosion barrier coating (CBC) to mitigate SiC corrosion rates [15] and act as a hermetic seal, preventing outward

loss of fission gas and H_2O ingress. However, there is a concern that Cr may disrupt the otherwise protective oxide formed on SiC during steam oxidation, as chromia formation is more rapid in steam than silica [8], and may negate the oxidation improvement of SiC/SiC ATF cladding. Furthermore, coating-substrate reaction products with un-desirable high temperature responses may form in the Cr-SiC system. Therefore, under LOCA conditions, reaction product formation and oxidation kinetics needs to be investigated.

In the present study, Cr coatings were deposited onto chemically vapor deposited (CVD) silicon carbide to simplify the study compared to coating a CMC substrate [16]. Most SiC/SiC CMCs have an outer dense CVD SiC seal coat such that the coating will be in contact with CVD SiC. Thermogravimetric analysis (TGA) was used to study steam oxidation from room temperature up to 1200°C and vacuum annealing was used to study reaction products in the absence of oxidation. As actual cladding temperatures are anticipated to increase beyond 1200°C during a beyond design basis accident, the present investigation is a preliminary study of the interaction of Cr and SiC in high temperature steam environments. While multiple reaction products were observed to form, no significant detrimental impact on the steam oxidation resistance of the Cr/SiC system was observed.

EXPERIMENTAL

Chromium coatings were deposited on CVD polycrystalline ß-SiC (Rohm and Haas) on all sides (10 mm x 20 mm x 2mm) using either high power impulse magnetron sputtering (HiPIMS) to form a nominally 5 µm thick coating (5HiPIMS), cathodic arc (CA) to deposit a nominally 10 µm thick coating (10CA), or the combination of both (5HiPIMS+10CA) with the 5HiPIMS deposited first for a nominally 15 µm thick coating. HiPIMS and CA are being currently being utilized as both processes bring different mechanical properties that are of interest to normal operation use. Specimens were cleaned with acetone prior to exposure, and specimen surface area was determined using digital Mitutoyo calipers (±0.01mm). Un-coated CVD SiC (10 mm x 20 mm x 2mm) were also prepared for steam exposure.

One set of coupons was vacuum annealed in a Brew furnace for 4 h at 1200°C with a pressure of ~10^{-4} Pa (10^{-6} Torr) to study reaction product formation in the absence of oxidation, while thermogravimetric analysis (TGA) was used to study the high temperature steam oxidation of another set of coupons. TGA was conducted with a Rubotherm Magnetic Suspension Balance TGA. Specimens were heated to 1200°C using the following profile: a 20°C/min ramp from room temperature to 550°C with flowing Ar followed by a 8 min hold while steam was introduced into the chamber at ~1.5 mL/h, with a gas velocity of ~ 1 cm/s. Temperature was then ramped at 20°C/min to 1200 ± 5°C, followed by a 4-h isothermal hold at 1200 ± 5°C. Once the hold was completed, steam flow was replaced with flowing argon while cooling to room temperature.

Specimen mounts were prepared by cross sectioning via low speed saw utilizing a diamond blade, embedding/fixturing with resin, and polishing. Back-scatter electron (BSE) scanning electron microscopy (SEM) and energy dispersive X-ray spectroscopy (EDS) were performed with a Tescan Mira3 FE-SEM operating at 20 kV. Au/Pd targets were used to sputter mounts prior to analysis. Post-exposure X-ray diffraction spectrum were run in 2θ-θ geometry with a Bruker D2Phaser diffractometer with a CuKα (λ=1.5406A) source and a LynxEye detector from 10-120°. MDI Jade and the PDF-4+ ICDD database were used for phase identification. Scale and layer thickness measurements from cross sectional images were performed with a semi-autonomous Python and ImageJ technique that allows thousands of measurements across large expanses of interfaces, limiting the subjective nature of individual

measurements. Reported thickness measurements were made across three 1-mm lengths of interface such that each individual thickness value reported is representative of 3-mm of total cross sectional length, totaling more than 3000 measurements per reported value.

RESULTS

Cross sectional BSE micrographs of as-received 5HiPIMS, 10CA, and 5HiPIMS+10CA coatings deposited onto SiC are shown in Figure 1(a-c), respectively. The 5HiPIMS and 5HiPIMS+10CA coatings were well adhered to the SiC substrate. In some regions, the 10CA coating was delaminated, with cracks running normal to the interface and terminating in the coating, seen in the inset of Figure 1(b). It's unclear if the cracks formed during deposition or sectioning. A darker grey contrast region was observed at the interface of the 10CA coating and the SiC substrate but was still identified to be Cr. Coating thicknesses were, respectively, 4.1 ± 0.2, 10.0 ± 0.4, and 12.9 ± 0.3 µm for the 5HiPIMS, 10CA, and 5HiPMS+10CA systems.

A cross sectional BSE micrograph of a 5HiPIMS specimen after vacuum annealing for 4-h at 1200°C is shown in Figure 2(a). Two reaction layers with well-defined interfaces were observed. EDS point quantification of three regions from each layer are reported in Table 1. Virtually no Si was found in the outer layer, while both Si and Cr were found in the inner layer. The presence of C was detected in both layers however a technique more sensitive to lighter elements, like electron probe microanalysis (EPMA), is needed to better quantify the C content. Regardless, EDS indicates a Cr_xC_y outer reaction layer and a $Cr_xSi_yC_z$ silicide inner reaction layer. Figure 2(b), an XRD result, also indicates $Cr_xSi_yC_z$ formation. There appeared to be a strong match to $Cr_xSi_yC_z$ (PDF# 00-009-0242) which shared many peaks with Cr_3Si (PDF# 04-003-1510) along with $CrSi_2$ (PDF# 04-004-7274). However, comparing the XRD spectra to the various Cr carbide phases available in the ICDD database, no clear match was found. The peaks in Figure 2(b) also did not match the XRD results of Naka [17]. No metallic Cr was detected but SiC peaks were present, indicating the entirety of the reaction layers were probed. Phase identification was complicated by the large number of reflections, low symmetry of the carbide and silicide phases, and high chances of peak overlap. Selective area electron diffraction may be necessary to isolate the different phases.

TGA specimen mass change for 5HiPIMS (red), 10CA (purple), 5HiPIMS+10CA (orange) and CVD SiC (green) during steam exposure from 550° to 1200°C followed by a 4 h hold is reported in Figure 3. Specimen mass gain determined via microbalance from initial and final specimen masses are also reported as single data points for comparison. TGA mass change for the uncoated CVD SiC specimen is not reported due to a low signal to noise ratio during the exposure. Compared to bare SiC, the mass gain was an order of magnitude larger for the Cr coated specimens. Up to the first ~0.5 h of exposure, mass gain between all the Cr coated SiC specimens were similar. After the initial mass gain, slight mass losses were observed for the HiPIMS and HiPIMS+CA specimens. The 10CA specimen exhibited the highest mass gain of the coated specimens. After removal, the coating was found to delaminate over large expanses (~25 mm^2) which may have increased the effective surface area.

Cross section BSE micrographs of all three Cr coated SiC specimens after steam exposure are shown in Figure 4(a-c). As can be seen, Cr coated SiC formed four distinct regions after 1200°C steam exposure: chromia at the ambient interface, a non-continuous region of Cr_xC_y, a $Cr_xSi_yC_z$ reaction layer underneath, and an interfacial Si and O rich layer. Layer thickness measurements are reported in Figure 5(a). The Cr_xC_y layer was taken as the entire length from the end of the Cr_2O_3 scale and the beginning of the $Cr_xSi_yC_z$ reaction product. Similar Cr_2O_3 and Cr_xC_y layer thicknesses were observed for all three specimens. However, the Cr_xC_y measurements do not include the observed discontinuities. The chromia appeared to

be comprised of two different regions with a discrete transition; a denser outer oxide and a more porous inner oxide. Thickness measurements of these regions are reported in Figure 5(b). The silicide reaction layer thickness increased with initial coating thickness.

A BSE cross section micrograph of the 5HiPIMS+10CA specimen after 1200°C steam exposure is shown in Figure 6(a) alongside associated EDS maps of O, Si, Cr, and C, Figure 6(b-e), respectively. As can be seen by comparing Figure 6(a) to Figure 4(a-c), the presently shown region is generally representative of all Cr coated specimens. At the gas interface, dense Cr_2O_3 forms, which transitions to a more porous chromia. XRD determined the oxide to be Cr_2O_3., Figure 7. Beneath the chromia scale, a non-continuous Cr_xC_y layer inter-dispersed with Si and O rich regions formed, followed by a $Cr_xSi_yC_z$ silicide layer. A Si and O rich interfacial layer with a thin (< 1µm) underlying Cr and C rich layer was observed to form between the carbide and silicide layers. The underlying Cr and C rich layer was relatively rich in O, indicating oxycarbide formation or dissolved oxygen. A BSE micrograph of a similar region from the 5HiPIMS specimen is shown in Figure 8(a), along with an EDS line scan profile with a 0.5 µm resolution running from the underlying SiC substrate and terminating in the chromia layer, Figure 8(b). The Si content decreased across the $Cr_xSi_yC_z$ reaction layer with a corresponding increase in Cr content towards the outside. The Cr content remained relatively constant across the carbide and oxide layers. Point quantification could not discern the Si and O rich interfacial layer, likely due to the thin feature thickness, < 300 nm, compared to the EDS interaction volume. Similar to the 1200°C vacuum annealed specimen, the Cr carbide regions here could not be indexed in the diffraction pattern, Figure 7. Prominent SiC peaks were observed, indicating the entirety of the reaction product layers were being probed. Again, the signal matched well with $Cr_xSi_yC_z$ phases.

A cross sectional BSE micrograph of the 10CA coated specimen in a delaminated region is shown in Figure 9(a). The length of detached interface is ~3.1 mm and the length of the detached segment is ~3.5 mm, which is approximately a 13% increase in length. The detached segment was 16.5 ± 1.5 µm in thickness and was entirely comprised of chromia – the original thickness of the 10CA coating was ~10µm. The coefficient of thermal expansion (CTE) of Cr has been reported to be ~15E-6 K^{-1} [18] and of ß-SiC to be ~5.2E-6 K^{-1} [19] at 1200°C, with a ~100% increase in volume during oxidation of Cr to Cr_2O_3. The observed increased length of the detached segment is potentially due to a combination of both these factors. A higher magnification BSE micrograph of the region where delamination began is shown Figure 9(b) and the location of the region is indicated by a dashed white rectangle in Figure 9(a). Associated EDS elemental maps of O, Si, Cr, and C are shown in Figure 9(c-f), respectively. Similar carbide and silicide reaction layers can be seen forming on the regions where the coating is still adhered, and the microstructure transitions to solely chromia further along the detached segment. A thin ~ 1 µm silica scale was observed to form on the regions where the coating detached, which is in good agreement with the oxidation rates reported by Opila [20] and indicates that the coating detached early in the exposure. Furthermore, no underlying Cr-Si reaction product is observed, indicating no coating-substrate interdiffusion occurred.

DISCUSSION

Carbide and silicide reaction products

Although the Cr-Si-C system is ternary, evaluation of the respective binary systems can provide insights into the observed reaction product formations. In the binary Cr-Si system, four silicides form: Cr_3Si, Cr_5Si_3, CrSi, and $CrSi_2$, all with melting/dissociation points well above 1200°C [21]: 1780°, 1666°, 1424°, and 1439°C, respectively [22]. In the Cr-C system, three carbides, $Cr_{23}C_6$, Cr_7C_3 and Cr_3C_2, form, also with

melting/dissociation points above 1200°C [23]: 1576°, 1766°, and 1811°C, respectively [24]. In the Cr_2O_3-SiO_2 system, no eutectics or compounds form [25]. Therefore, the multilayered microstructure that is presently observed to form, Figure 4, is solely the result of oxidation and interdiffusion, with no eutectic, liquid-solid, or liquid-liquid phase interaction anticipated.

As can be seen in Figure 2, oxidation is not necessary to form the Cr_xC_y and $Cr_xSi_yC_z$ reaction layers. Kung reported similar microstructural formations during the fabrication of chromium-carbide conversion coatings on SiC [26]. Carbide-silicide reaction layers with well-defined interfaces were observed, with both the carbide and silicide layers each being comprised of sublayers: EPMA revealed $Cr_{23}C_6/Cr_7C_3/Cr_3C_2$ followed by $Cr_3Si/Cr_5Si_3C_x/SiC$. The presently reported reaction layers may be similar, but the conversion process Kung used was conducted at 1250°C over the course of 30 h under flowing argon and may be more representative of equilibrium conditions. More experimentation specifically aimed at obtaining the rates of carbide and silicide formation during transient and isothermal temperatures are necessary to model the reaction process.

Oxidation

Tedmon observed Cr to oxidize,

$$2Cr + 3/2\ O_2\ (g) \rightarrow Cr_2O_3 \qquad (1)$$

in a parabolic manner over the temperature range of 1000-1300°C, [27]. Cr oxidation has been found to be independent of oxygen partial pressure [28]. Small amounts of water vapor have been shown to accelerate Cr oxidation,

$$2Cr + 3H_2O\ (g) \rightarrow Cr_2O_3 + 3H_2\ (g) \qquad (2)$$

by relatively small amounts [18, 19, 20]. For Fe-Cr alloys with lower amounts of Cr, wet oxygen generally increases oxidation rates by more than an order of magnitude after initial periods of protective oxidation [29], as volatilization of Cr_2O_3 in wet oxygen [30–33],

$$½Cr_2O_3 + H_2O\ (g) + ¾O_2\ (g) \rightarrow CrO_2(OH)_2\ (g) \qquad (3)$$

can reduce the Cr concentration of the underlying alloy beneath a critical content. Once below this threshold, less protective iron oxide formation begins to occur [34]. In pure steam, however, oxygen partial pressure is low, Eq 3, and chromia volatility is anticipated to be low [32]. Furthermore, for a metallic Cr coating, there is no potential to form less protective iron oxide.

There is little information regarding the impact of high steam partial pressures on chromia formation at high temperatures. Tedmon calculated a parabolic rate constant of ~1.08 mg^2/cm^4h for the 1200°C oxidation of Fe-95Cr in O_2 at 1.3E-4 MPa [27], while Pint et al. determined a parabolic rate constant of 0.72 mg^2/cm^4h for chromia formation on 310SS at 1200°C in Ar-50%H_2O at 1 bar [9]. To determine rate constants, specimen mass gain data from Figure 3 was truncated so that t = 0 h when T ~1195°C. Truncated specimen mass gain is plotted against $t^{1/2}$ in Figure 10, such that

$$\Delta w = (k_p t)^{1/2} \qquad (4)$$

where Δw is mass gain in units of mg/cm^2, k_p is the parabolic rate constant in units of mg^2/cm^4h, and t is exposure time in h. The slopes are equivalent to $k_p^{1/2}$ and R^2 values indicate the degree of fit to parabolic behavior. As can be seen, mass gain was fairly parabolic during initial exposure, with rate constants of

0.52, 0.76, and 0.74 mg^2/cm^4h for the 5HiPIMS, 10CA, and 5HiPIMS+10CA coating, respectively, all with R^2 values above 0.99. These are roughly the same in value as the rate constant of 0.72 mg^2/cm^4h determined by Pint et al. during 1200°C steam oxidation of 310SS in Ar-50%H_2O [9]. The equivalence is not viewed as mechanism agreement. Rather, it's an indication that steam oxidation of Cr potentially occurs at similar rates to those of chromia forming alloys. Similarly, the presently determined rate constants are lower than those observed by Tedmon but is not an indication that oxidation of Cr is slower in steam. Rather, that the impact of steam on Cr oxidation may not be as profound or as significant as that observed in other systems, for instance, the order of magnitude increase in silica formation [35]. A second parabolic oxidation regime may exist for the Cr coated specimens, as indicated by the linear appearance of mass change after the initial parabolic regime in Figure 10. The data could not be fit well but may be due to the large degree of noise.

The transition from dense to porous chromia, Figure 4, Figure 5(b), and Figure 6, could be an indication that chromia formation is not due solely to metallic Cr oxidation. Using a density of 7.14 g/cm^3 for Cr and assuming a density of 6.68 g/cm^3 for Cr carbide, there is a ~100% volume expansion during the oxidation of Cr compared to a 61% volume expansion during oxidation of Cr_3C_2. A transition from metallic to carbide oxidation could result in a more porous scale forming, but the porosity could also be due to a diffusional imbalance.

Using calculated rate constants from Figure 10, mass gain due to 1200°C Cr oxidation in steam can be projected using Eq 4. As previously discussed, in steam the partial pressure of O_2 is anticipated to be low and chromia volatilization negligible. Assuming stoichiometric oxidation, projected specimen mass gain, chromia scale thickness evolution, and Cr consumption during 1200°C exposure using k_p = 0.76 mg^2/cm^4h are shown in Figure 11. Across all three Cr coated samples, the average thickness of total formed chromia was ~7 µm, and the average thickness of the denser outer chromia layer was ~5.5 µm, Figure 5(b). From Figure 11, 7 µm of chromia formation consumes ~3.5 µm of Cr after 1.74 h, while 5.5 µm of chromia formation consumes ~2.7 µm of Cr after 1.06 h. Therefore, it is unlikely that chromia formation occurs solely to metallic Cr oxidation, as the 7 µm scale is anticipated to form after only 1.74 h - actual mass change was observed to increase throughout the entire 1200°C hold beyond 1.74 h, Figure 3, indicating continued oxide formation. It's possible that after 7 µm of chromia formation from metallic Cr, oxidation of the underlying Cr_xC_y layer occurs at a rate low enough for additional chromia formation to be negligible. However, it's also possible that 2.7 µm of metallic Cr was consumed to form a dense 5.5 µm layer of chromia after 1.06 h and that subsequent chromia formation occurs at the expense of the underlying reaction layers.

The presently conducted steam exposures were not isothermal though, as steam was present during the temperature ramp. It's probable that a non-negligible extent of Cr oxidation occurred during the temperature transient, and thus, the projected times of chromia formation in Figure 11 are over-estimated. Regardless, the comparison between observed formation and projected formation does provide an estimate of Cr consumption due to oxidation, even with the potential transition from metallic Cr to Cr carbide oxidation; ~ 2.8-3.5 µm of the Cr coating is consumed due to steam oxidation. The remaining metallic Cr is consumed by formation of the Cr carbide and silicide reaction product layers. Evaluation of the Cr carbide layer thickness, Figure 5(b), revealed no significant differences between the different coating thicknesses, while statistically significant differences were observed for the silicide layer. The non-continuous nature and potential oxidation may be obfuscating thickness measurements of the

carbide layer, as the formation of the silicide and carbide layer are anticipated to be correlated, and therefore thicker silicide layers should be accompanied by thicker carbide layers.

The Si and O rich regions, shown in Figure 6 for the 5HiPIMS+10CA specimen but observed to form in all coated specimens, is an indication of silica formation. These regions occur in two distinct manners: at the carbide-silicide interface and inter-dispersed within the Cr carbide layer. At the carbide-silicide interface, Si selectively oxidizes for form silica. Accordingly, Cr rich regions were observed underlying the interface with no Cr_2O_3 formation apparent. Cr_3Si is thought to have a similar high temperature oxidation resistance to that of $MoSi_2$ under both isothermal [36] and cyclic [37] conditions. Raj reported on the oxidation resistance of $Cr_{40}Mo_{30}Si_{30}$ [38] and observed that the alloy formed two protective oxide scales, consisting primarily of Cr_2O_3 below 1000 K and purely SiO_2 above 1575 K. Tomasi et al. reported a similar scale morphology transition for a lower Mo content Cr silicide [39]. 1200°C oxidation of silica formers in wet conditions have been reported to be rate limited by molecular diffusion through amorphous silica [4,40]. Silica formation occurs as,

$$Si + 2H_2O(g) \rightarrow SiO_2 + 2H_2(g) \qquad (5).$$

Cross sections revealed scale spanning cracks that run normal to the formed interfaces, Figure 4. If present at high temperatures, the cracks would provide direct transport of oxidants to the silicide layer. The cracks may also form upon cooling due to coefficient of thermal expansion mismatch between all the layers and may not be present at temperature. If so, diffusion of oxidants through the chromia and Cr carbide layer would be necessary to form silica at the carbide/silicide interface. The mechanisms of silica formation remain to be elucidated. What is clear is that the Si and O rich regions do not form after annealing, Figure 2, and are a direct consequence of steam oxidation. Silica formation is anticipated to be slow compared to chromia formation and therefore contribute little to mass gain or hydrogen production.

Examination of the delaminated region, Figure 9, provides some insight into silica formation in the coating. The region presented in Figure 9(b) represents a transition from free standing to fully adhered Cr coating and the respective differences in evolved microstructure during steam exposure. Starting on the fully detached segment on the right, the composition is solely Cr and O. Then, in the middle of the segment, a small silica region is observed that transitions to the lighter shades of grey associated with the carbide and silicide phases. On the left of Figure 9(b), where the coating has remained fully adhered, the general four layer reaction product formation shown in Figure 4 andFigure 6 is seen. Specifically, a relatively large amount of silica is observed between the chromia and carbide layers, and the amount of silica decreases in the direction where the coating has begun to delaminate. Based on the cross section alone, it cannot be concluded at which point during the exposure delamination occurred but the thin layer of Cr_xC_y, Figure 9(e), that extends from the fully adhered segments of the coating into the delaminated regions indicate some degree of interdiffusion occurred prior to delamination. At the end of this segment, silica formation is observed. It is difficult to draw many conclusions from a single phenomenon.

Comparative rates of hydrogen generation

Based on this preliminary study, no detrimental reaction product formation occurs during the steam oxidation of Cr coated SiC up to 4 h at 1200°C. Rates of mass gain, and consequently of hydrogen gas production, are still ~100x slower than zirconium based claddings. Projected mass gain during 1200°C steam oxidation of various cladding materials is shown in Figure 12(a), utilizing Eq 4 and reported parabolic

rate constants [1,5,9]. The oxide for each cladding is shown in the legend, and hydrogen gas production is estimated in Figure 12(b) assuming stoichiometric oxidation for each oxide as

$$Zr + 2H_2O\ (g) \rightarrow ZrO_2 + 2H_2\ (g) \quad (6)$$

$$2Cr + 3H_2O\ (g) \rightarrow Cr_2O_3 + 3H_2\ (g) \quad (7)$$

$$2Al + 3H_2O\ (g) \rightarrow Al_2O_3 + 3H_2\ (g) \quad (8)$$

$$SiC + 3H_2O\ (g) \rightarrow SiO_2 + 3H_2 + CO\ (g) \quad (9)$$

during 4-h of 1200°C isothermal steam exposure. A rate constant of 0.76 mg^2/cm^4h has been used for the presently reported Cr coatings. This was the highest rate constant observed amongst the three coating systems, Figure 10. While mass gain was not observed to be governed by a single parabolic rate constant throughout exposure, predicted mass gain after 4 h at 1200°C using a single rate constant was ~1.8 mg/cm^2, Figure 12(a), while the highest observed mass gain after 4.5 h of 1200°C steam TGA exposure (~0.5 h temperature ramp and 4 h of 1200°C isotherm) was ~1.5 mg/cm^2, Figure 3. The transition from metallic Cr to carbide oxidation, Eq 5, could result in a 2 fold increase in H_2 generation on a mol per gram mass gain basis, 0.0625 mol H_2/gcm^{-2} compared to 0.135 mol H_2/gcm^{-2}, respectively. As previously discussed, the transition would be anticipated to occur no later than 1.06 – 1.74 h into the 1200°C isotherm. The largest mass gain, in all three coated specimens, occurring after this transition time is ~0.2 mg/cm^2 (observed for the 5HiPIMS+10CA and 10CA coatings); 0.2 mg/cm^2 is 10-20% of the mass gain for each Cr coated specimen. This would translate into a 23.2% maximum increase in H_2 production, ~1.2E-4 mol H_2/cm^2 to 1.48E-4 mol H_2/cm^2, after 4.5 h of 1200°C isotherm. This is a 34 fold decease compared to the estimated 4.77E-3 mol H_2/cm^2 production during steam oxidation of Zr-based cladding assuming parabolic oxidation.

It's important to draw a distinction between the anticipated role of Cr in the incumbent Zr-based cladding system and in the proposed SiC-based composite cladding system. For the former, Cr coatings bestow accident tolerance, while in the latter Cr coatings would grant normal operational tolerance i.e. composite hermeticity. In accident modelling work reported by Feng *et al.*, it was shown that while a Cr coating can delay hydrogen production in the Zr-based system, the delay does not significantly change the total amount of hydrogen produced [41]. Brachet *et al.* reported that up to temperatures of 1300°C, oxidation of Cr coated Zr is initially nearly parabolic but transitions to non-protective behavior [42,43]. Above 1300°C, eutectic formation in the Zr-Cr binary system is anticipated to have a deleterious effect. This may be in stark contrast with the Cr coated SiC system, where upon complete Cr consumption, oxidation rate decreases, at least up to 1200°C, Figure 3. Future work on Cr coated SiC will need to focus on higher temperatures, as there are several eutectics in the binary systems. In the Cr-Si system, eutectic formations are anticipated at 1701°, 1408°, and 1328°C [22], while in the Cr-C system, eutectic formations are anticipated at 1534° and 1727°C [24].

SUMMARY AND CONCLUSIONS

Chromium was deposited onto CVD SiC with HiPIMS, CA, and the combination of both, to nominal thicknesses of 5, 10, and 15 µm, respectively. As expected, all coating-substrate systems formed two reaction layers after 1200°C vacuum annealing, a Cr carbide layer and a $Cr_xSi_yC_z$ layer. Similar reaction products formed after 1200°C steam exposures but with a thick Cr_2O_3 outer scale forming and a Si and O rich interfacial region forming between the carbide and silicide reaction products. The HiPIMS and

HiPIMS+CA coatings were well adhered after steam exposure, but large expanses of the CA coated specimen were delaminated. A transition from a dense to a more porous chromia microstructure was observed in all coated specimens after steam exposure. Although less oxidation resistant than uncoated SiC, Cr coatings were fully consumed by oxidation and interdiffusion with the SiC at 1200°C and then the rate slowed significantly, perhaps controlled by an inner SiO_2 layer. The H production will still be significantly lower than current Zr-based alloy cladding.

Acknowledgements

The authors would like to thank B. Johnsons and M. Howell for their technical assistance, to T. Geer for their metallography expertise, and to Y. Katoh for helpful comments. Coatings were deposited by by Acree Technologies (Concord, CA). The research is sponsored by the Advanced Fuels Campaign of the Nuclear Technology Research and Development Program, Office of Nuclear Energy, Department of Energy (DOE), and Westinghouse Electric Company/General Atomics FOA program, under contract DE-AC05-00OR22725 with UT-Battelle LLC.

FIGURES

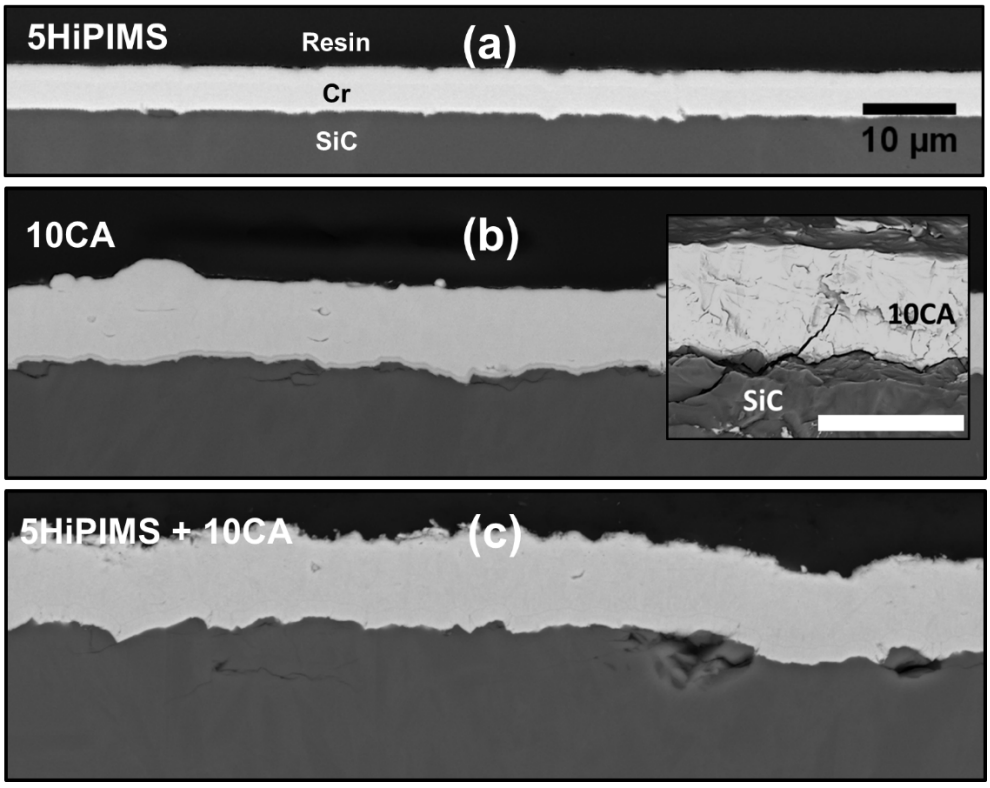

Figure 1 Cross sectional BSE micrograph of the (a) 5HiPIMS, (b) 10CA, and (c) 5HiPIMS+10CA Cr coatings deposited onto SiC.

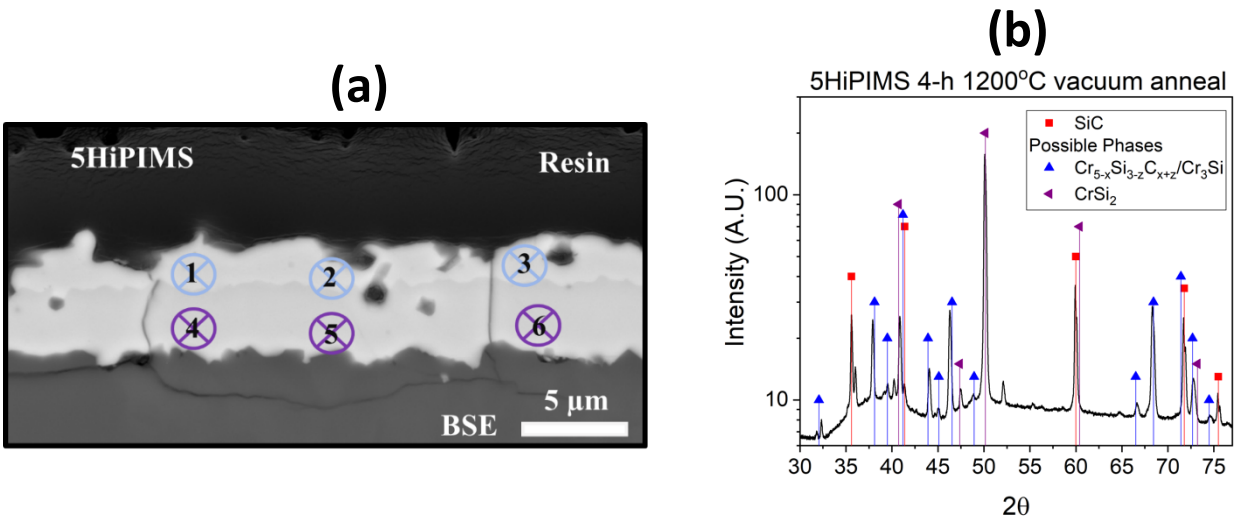

Figure 2 (a) Cross sectional BSE of the reaction layers that formed in a 5HiPIMS specimen after 4-h vacuum annealing at 1200°C. The 5HiPIMS+10CA system and 10CA systems formed similar reaction products. (b) XRD pattern obtained from the same 5HiPIMS specimen prior to cross sectioning.

Table 1 EDS quantification of three points from each reaction layer shown in Figure 2.

Point	Cr (at%)	Si (at%)	C (at%)
1	53	-	47
2	51	1	48
3	48	2	50
4	44	27	29
5	44	27	29
6	44	27	29

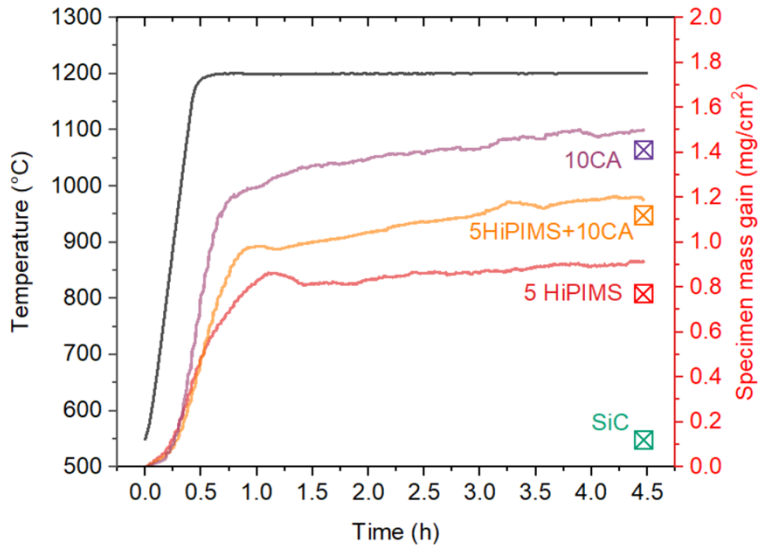

Figure 3 TGA specimen mass gain during 1200°C exposure. Steam was introduced at ~550°C. Due to a low signal to noise ratio, SiC TGA mass gain is not plotted. Single data point mass gains are reported for the coated and bare SiC and were determined via microbalance from initial and final mass.

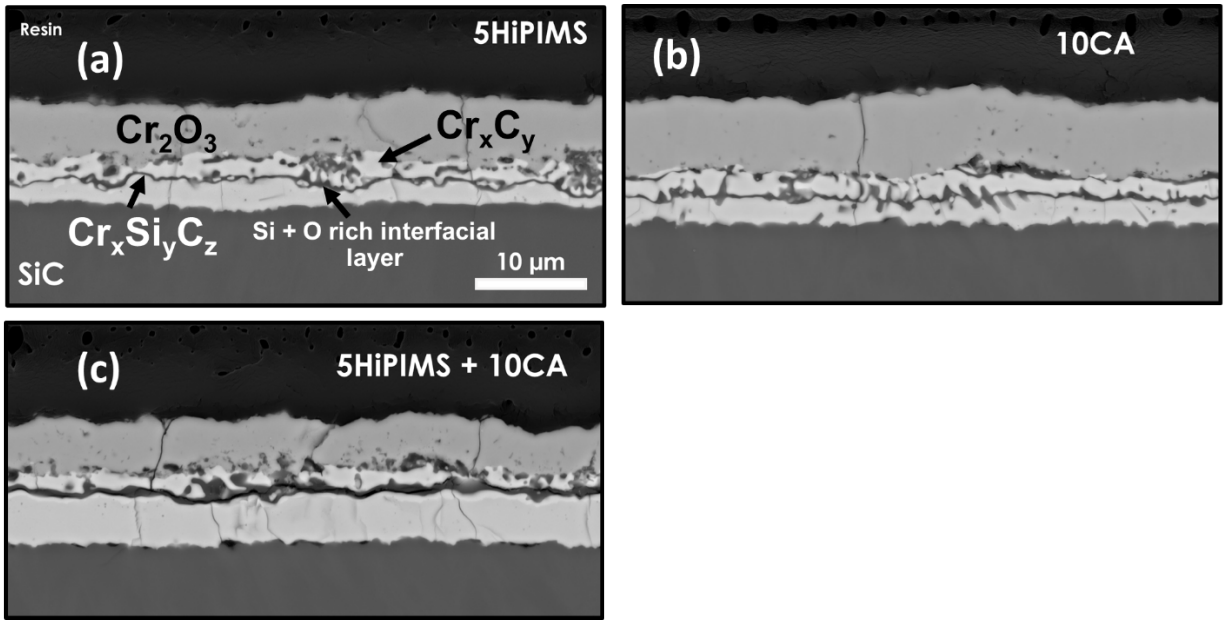

Figure 4 Cross section BSE micrographs of the (a) 5HiPIMS, (b) 10CA, and (c) 5HiPIMS+10CA coating systems after 1200°C steam exposure.

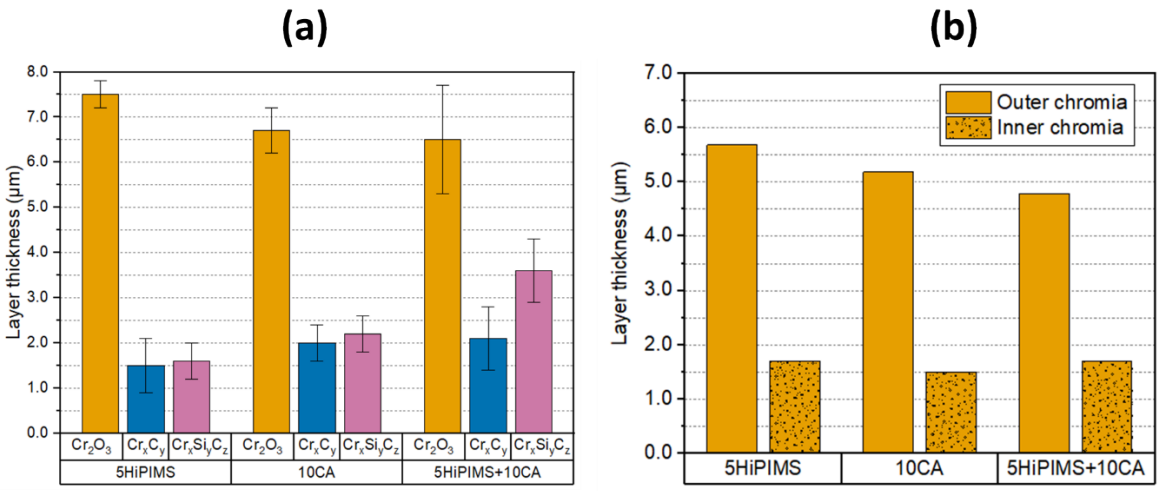

Figure 5 (a) Thickness measurements of the Cr_2O_3, Cr_xC_y, and $Cr_xSi_yC_z$ layers that form after 4-h of steam exposure at 1200°C for the 5HiPIMS, 10CA, and 5HiPIMS+10CA systems. The Cr_xC_y layer is taken as the entire length from the end of the Cr_2O_3 oxide scale to the beginning of the $Cr_xSi_yC_z$ reaction product layer. The Cr_xC_y layer was found to be discontinuous in some regions, and aforementioned automated scale analysis code was programmed to exclude these regions. Initial coating thicknesses were 4.1 ± 0.2, 10.0 ± 0.4, and 12.9 ± 0.3 µm for the 5HiPIMS, 10CA, and 5HiPMS+10CA systems. (b) Thickness measurements of the dense, outer region of the Cr_2O_3 layers and the porous, inner regions.

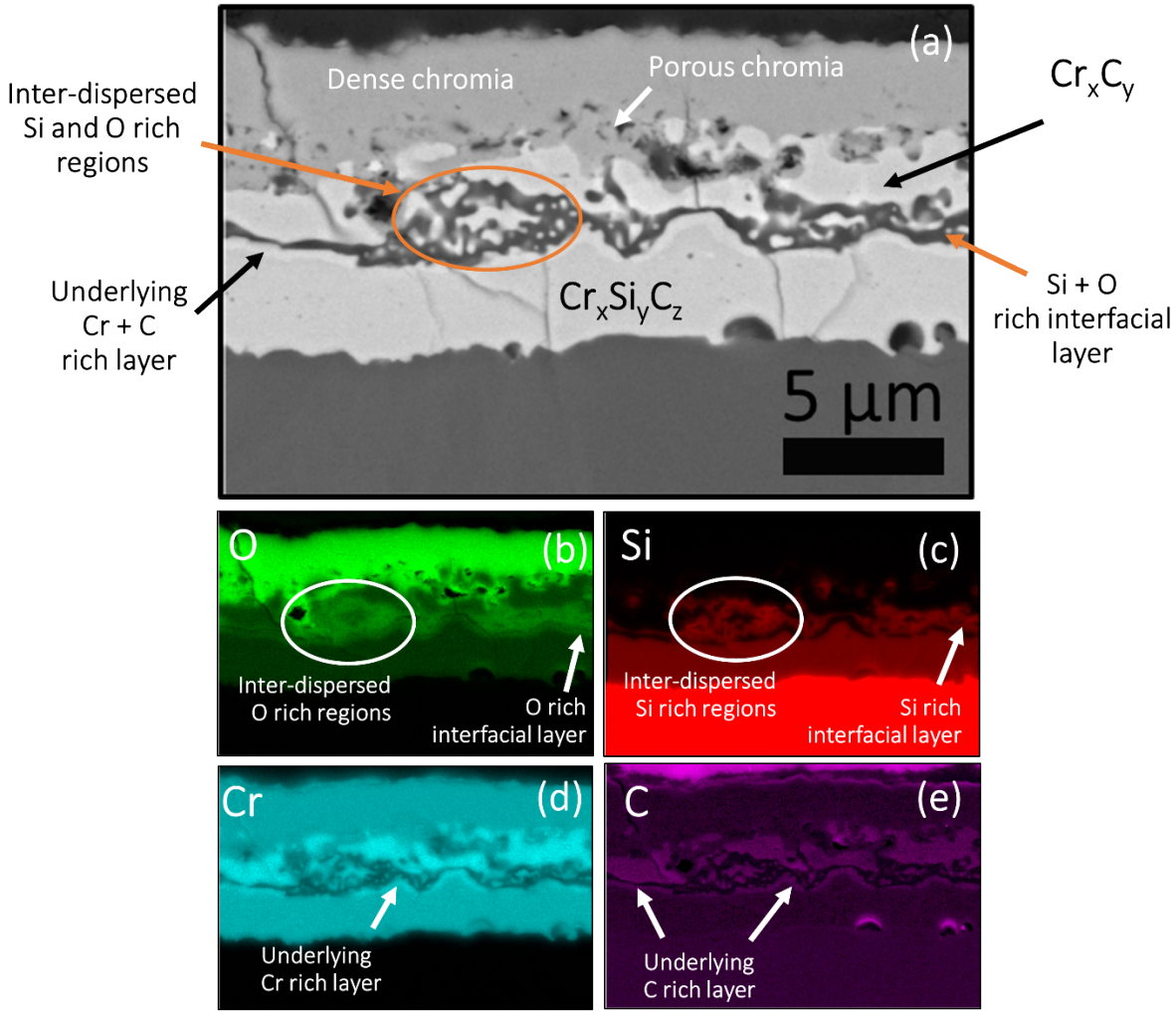

Figure 6 Cross section BSE micrograph of the (a) 5HiPIMS+10CA system after 1200°C steam exposure, and EDS maps of, respectively, (b-e) oxygen, silicon, Cr, and carbon. The 5HiPIMS and 10CA systems formed similar regions.

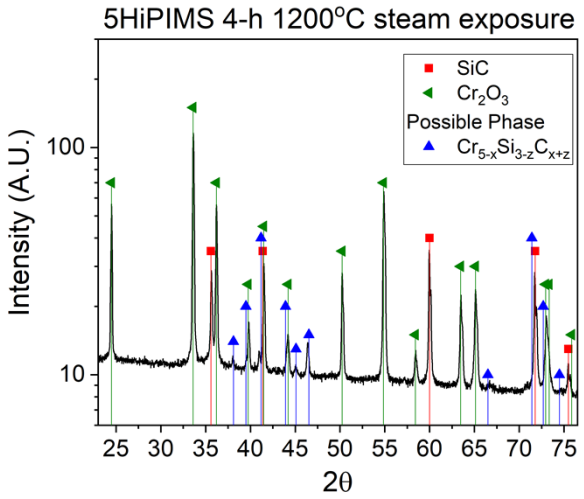

Figure 7 XRD patterns obtained from a 5HiPIMS specimen after steam exposure from room temperature up to 1200°C followed by a 4-h hold. XRD patterns obtained from the 5HiPIMS+10CA were similar.

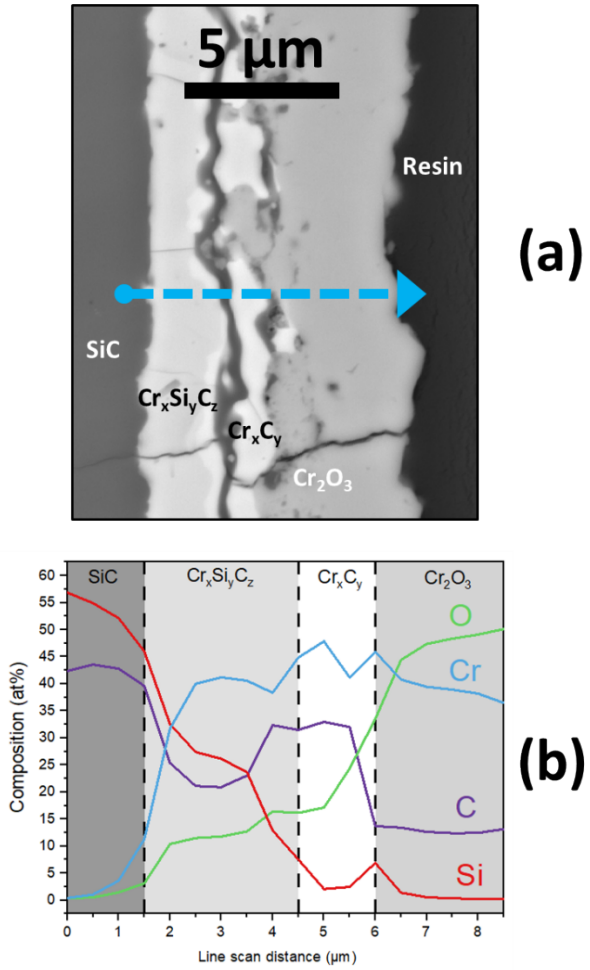

Figure 8 (a) Cross section BSE micrograph of the 5HiPIMS specimen after 1200°C steam exposure and (b) associated EDS line scan profile with a 0.5 µm resolution.

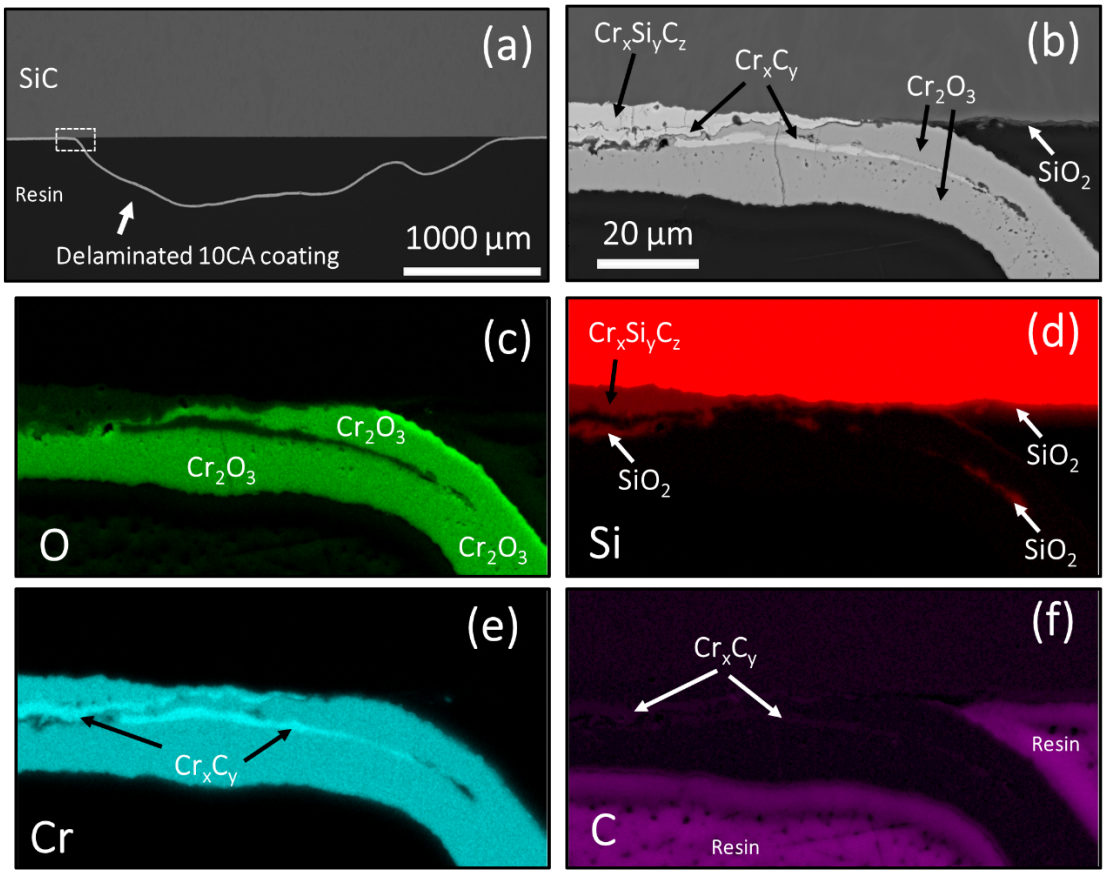

Figure 9 (a) BSE micrograph of a cross section taken from the 10CA sample in a region of coating delamination after 1200°C steam exposure. (b) Magnified BSE micrograph of the region where delamination occurs, location is marked by dashed rectangle in (a). Elemental EDS maps of (c) oxygen, (d) silicon, (e) Cr, and (f) carbon.

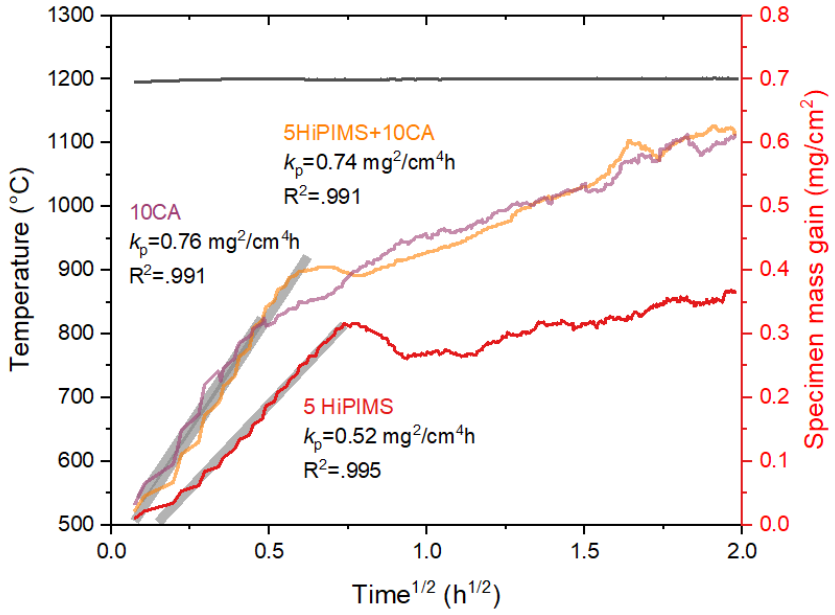

Figure 10 Specimen mass gain plotted against the square root of time for 5HiPIMS (red), 10CA (purple), 5HiPIMS+10CA (orange) from Figure 3, but truncated such that when T ~1195°C, t = 0 h, and mass gain is zero.

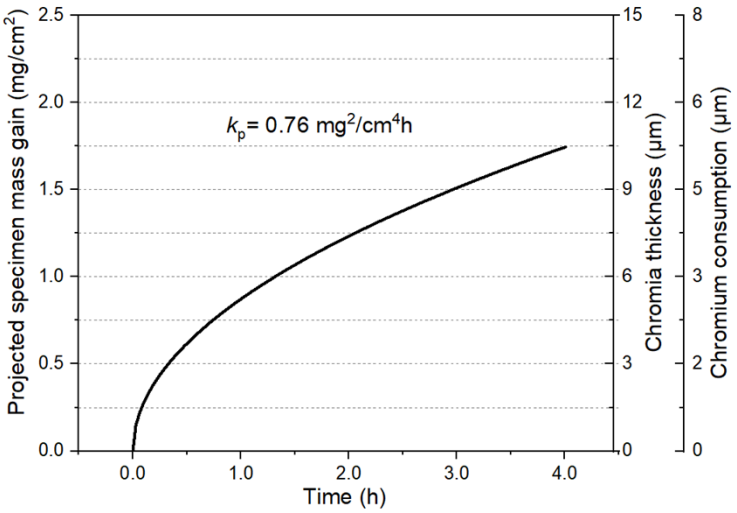

Figure 11 Projected specimen mass gain, chromia formation, and Cr consumption with time at 1200°C based off the largest rate constant observed during the 1200°C steam isotherm. Chromia thickness is calculated assuming stoichiometric oxidation, for every 48 g of mass gain 1 mol of Cr_2O_3 forms, and a chromia density of 5.22 g/cm^3. Chromium consumption is calculated based on every 1 mol of Cr_2O_3 formation, 104 g of Cr is consumed.

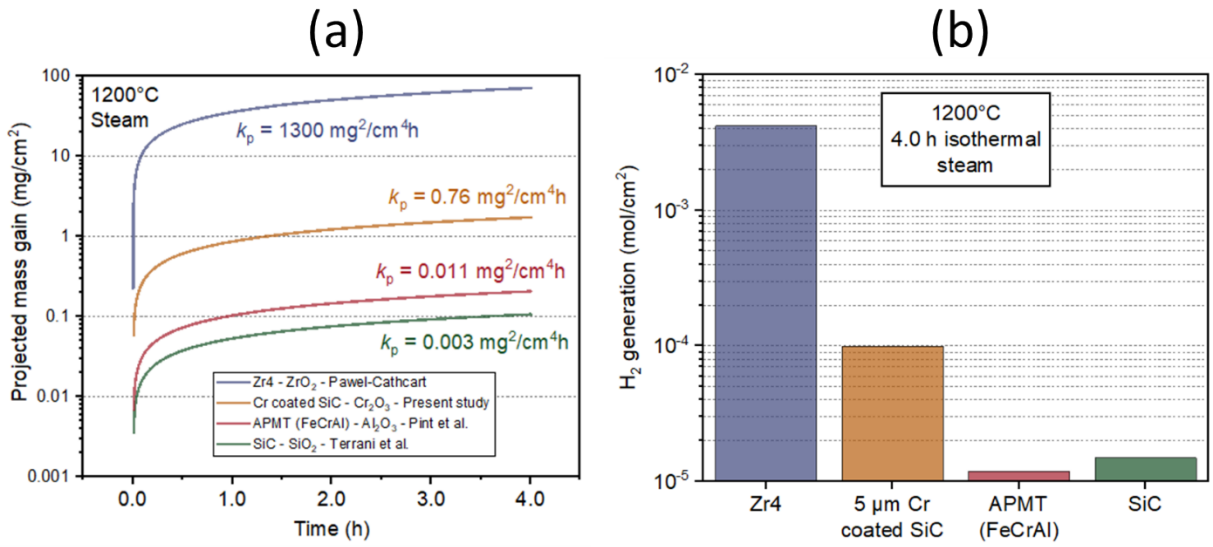

Figure 12 (a) Projected mass gain of various cladding materials during isothermal 1200°C steam oxidation [1,5,9] *(b) Estimated hydrogen generation assuming stoichiometric oxidation of cladding materials in (a).*

REFERENCES

[1] J. V Cathcart, R.E. Pawel, R.A. McKee, R.E. Druschel, G.J. Yurek, J.J. Campbell, S.H. Jury, Zirconium metal-water oxidation kinetics. IV. Reaction rate studies, Oak Ridge National Lab., 1977.

[2] S.J. Zinkle, K.A. Terrani, J.C. Gehin, L.J. Ott, L.L. Snead, Accident tolerant fuels for LWRs: A perspective, J. Nucl. Mater. 448 (2014) 374–379. doi:10.1016/j.jnucmat.2013.12.005.

[3] F.J. Erbacher, S. Leistikow, Zircaloy fuel cladding behavior in a loss-of-coolant accident: a review, in: Zircon. Nucl. Ind., ASTM International, 1987.

[4] E.J. Opila, Oxidation Kinetics of Chemically Vapor-Deposited Silicon Carbide in Wet Oxygen, J. Am. Ceram. Soc. 77 (1994) 730–736. doi:10.1111/j.1151-2916.1994.tb05357.x.

[5] K.A. Terrani, B.A. Pint, C.M. Parish, C.M. Silva, L.L. Snead, Y. Katoh, Silicon carbide oxidation in steam up to 2 MPa, J. Am. Ceram. Soc. 97 (2014) 2331–2352. doi:10.1111/jace.13094.

[6] K. Hironaka, T. Nozawa, T. Hinoki, N. Igawa, Y. Katoh, L.L. Snead, A. Kohyama, High-temperature tensile strength of near-stoichiometric SiC/SiC composites, J. Nucl. Mater. 307 (2002) 1093–1097.

[7] K. Shimoda, T. Hinoki, H. Kishimoto, A. Kohyama, Enchanced high-temperature performances of SiC/SiC composites by high densification and crystalline structure, Compos. Sci. Technol. 71 (2011) 326–332.

[8] K.A. Terrani, Accident tolerant fuel cladding development: Promise, status, and challenges, J. Nucl. Mater. 501 (2018) 13–30. doi:10.1016/j.jnucmat.2017.12.043.

[9] B.A. Pint, K.A. Terrani, M.P. Brady, T. Cheng, J.R. Keiser, High temperature oxidation of fuel cladding candidate materials in steam-hydrogen environments, J. Nucl. Mater. 440 (2013) 420–

427. doi:10.1016/j.jnucmat.2013.05.047.

[10] K. Yueh, K.A. Terrani, Silicon carbide composite for light water reactor fuel assembly applications, J. Nucl. Mater. 448 (2014) 380–388.

[11] Y. Katoh, L.L. Snead, C.H. Henager, T. Nozawa, T. Hinoki, A. Iveković, S. Novak, S.M. Gonzalez De Vicente, Current status and recent research achievements in SiC/SiC composites, J. Nucl. Mater. 455 (2014) 387–397. doi:10.1016/j.jnucmat.2014.06.003.

[12] C.P. Deck, G.M. Jacobsen, J. Sheeder, O. Gutierrez, J. Zhang, J. Stone, H.E. Khalifa, C.A. Back, Characterization of SiC-SiC composites for accident tolerant fuel cladding, J. Nucl. Mater. 466 (2015) 667–681. doi:10.1016/j.jnucmat.2015.08.020.

[13] L.H. Alva, X. Huang, G.M. Jacobsen, C.A. Back, High Pressure Burst Testing of SiCf-SiCm Composite Nuclear Fuel Cladding, in: H. Jin, C. Sciammarella, S. Yoshida, L. Lamberti (Eds.), Adv. Opt. Methods Exp. Mech. Vol. 3, Springer International Publishing, Cham, 2015: pp. 387–393.

[14] M. Wagih, B. Spencer, J. Hales, K. Shirvan, Fuel performance of chromium-coated zirconium alloy and silicon carbide accident tolerant fuel claddings, Ann. Nucl. Energy. 120 (2018) 304–318. doi:10.1016/j.anucene.2018.06.001.

[15] C. Ang, Y. Katoh, C. Kemery, J. Kiggans, K. Terrani, Chromium-Based Mitigation Coatings on SiC Materials for Fuel Cladding, Transactions. 114 (2016) 1095–1097.

[16] Y. Lee, T. Koyanagi, B.A. Pint, Y. Kato, High temperature steam oxidation of Cr-coated SiCf/SiC composite for LWR cladding applications, Oak Ridge National Lab.(ORNL), Oak Ridge, TN (United States), 2019.

[17] M. Naka, J.C. Feng, J.C. Schuster, Phase reactions and diffusion path of the SiC/Cr system, J. Mater. Synth. Process. 6 (1998) 169–173.

[18] N.A. Dubrovinskaia, L.S. Dubrovinsky, S.K. Saxena, B. Sundman, Thermal expansion of chromium (Cr) to melting temperature, Calphad Comput. Coupling Phase Diagrams Thermochem. 21 (1997) 497–508. doi:10.1016/S0364-5916(98)00007-8.

[19] Z. Li, R.C. Bradt, Thermal expansion of the cubic (3C) polytype of SiC, J. Mater. Sci. 21 (1986) 4366–4368. doi:10.1007/BF01106557.

[20] E.J. Opila, Variation of the Oxidation Rate of Silicon Carbide with Water-Vapor Pressure, J. Am. Ceram. Soc. 82 (2004) 625–636. doi:10.1111/j.1151-2916.1999.tb01810.x.

[21] F.A. Shunk, Constitution of binary alloys: second supplement, McGraw-Hill, 1969.

[22] H. Okamoto, Cr-Si (chromium-silicon), J. Phase Equilibria. 22 (2001) 593.

[23] T.B. Massalski, Binary alloy phase diagrams, ASM Int. 3 (1992) 2874.

[24] M. Venkatraman, J.P. Neumann, The C-Cr (Carbon-Chromium) System, Bull. Alloy Phase Diagrams. 11 (1990) 152–159. doi:10.1007/BF02841701.

[25] P.L. Roeder, F.P. Glasser, E.F. Osborn, The System Al2O3-Cr2O3-Sio2, J. Am. Ceram. Soc. 51 (1968) 585–593.

[26] S.C. Kung, Formation of a chromium-carbide conversion coating on silicon carbide, Oxid. Met. 42 (1994) 191–203. doi:10.1007/BF01052022.

[27] C.S. Tedmon, The High-Temperature Oxidation of Fe-Cr Alloys in the Composition Range of 25–95% Cr, J. Electrochem. Soc. 114 (1967) 788. doi:10.1149/1.2426737.

[28] P. Kofstad, K.P. Lillerud, On high temperature oxidation of chromium: II. Properties of and the oxidation mechanism of chromium, J. Electrochem. Soc. 127 (1980) 2410.

[29] S.R.J. Saunders, M. Monteiro, F. Rizzo, The oxidation behaviour of metals and alloys at high temperatures in atmospheres containing water vapour: A review, Prog. Mater. Sci. 53 (2008) 775–837. doi:10.1016/j.pmatsci.2007.11.001.

[30] C.S. Tedmon Jr, The effect of oxide volatilization on the oxidation kinetics of Cr and Fe-Cr alloys, J. Electrochem. Soc. 113 (1966) 766.

[31] E.J. Opila, Volatility of common protective oxides in high-temperature water vapor: current understanding and unanswered questions, in: Mater. Sci. Forum, Trans Tech Publ, 2004: pp. 765–774.

[32] D.J. Young, B.A. Pint, Chromium volatilization rates from Cr2O3 scales into flowing gases containing water vapor, Oxid. Met. 66 (2006) 137–153. doi:10.1007/s11085-006-9030-1.

[33] A. Yamauchi, K. Kurokawa, H. Takahashi, Evaporation of Cr 2 O 3 in atmospheres containing H 2 O, Oxid. Met. 59 (2003) 517–527. doi:10.1023/A:1023671206976.

[34] W.J. Quadakkers, J. Żurek, M. Hänsel, Effect of water vapor on high-temperature oxidation of FeCr alloys, J. Mater. 61 (2009) 44–50.

[35] E.J. Opila, Variation of the Oxidation Rate of Silicon Carbide with Water-vapor pressure, J. Am. Ceram. Soc. 82 (1999) 625–636.

[36] E.A. Aitken, J.H. Westbrook, Intermetallic compounds, Corros. Behav. Intermet. Compd. New York John Wiley Sons, Inc. (1967) 491–515.

[37] D.L. Anton, D.M. Shah, Proceedings of International Symposium on Intermatallic Compounds-Structure and Mechanical Properties (JIMIS-6), in: O. Izumi (Ed.), The Japan Institute of Metals, 1991: p. 379.

[38] S. V. Raj, An evaluation of the properties of Cr3Si alloyed with Mo, Mater. Sci. Eng. A. 201 (1995) 229–241. doi:10.1016/0921-5093(95)09767-8.

[39] A. Tomasi, R. Ceccato, M. Nazmy, S. Gialanella, Microstructure and oxidation behaviour of chromium-molybdenum silicides, Mater. Sci. Eng. A. 239–240 (1997) 877–881. doi:10.1016/s0921-5093(97)00678-3.

[40] B.E. Deal, A.S. Grove, General relationship for the thermal oxidation of silicon, J. Appl. Phys. 36 (1965) 3770–3778. doi:10.1063/1.1713945.

[41] T. Feng, J. Wang, Y. Zhou, P. Song, M. Wang, R. Dailey, W. Tian, M.L. Corradini, Quantification of the effect of Cr-coated-Zircaloy cladding during a short term station black out, Nucl. Eng. Des. 363 (2020) 110678. doi:10.1016/j.nucengdes.2020.110678.

[42] J.C. Brachet, M. Le Saux, M. Le Flem, S. Urvoy, E. Rouesne, T. Guilbert, C. Cobac, F. Lahogue, J. Rousselot, M. Tupin, P. Billaud, C. Hossepied, F. Schuster, F. Lomello, A. Billard, G. Velisa, E. Monsifrot, J. Bischoff, A. Ambard, On-going studies at CEA on chromium coated zirconium based nuclear fuel claddings for enhanced Accident Tolerant LWRs Fuel, TopFuel. (2015) 31–38.

[43] J.C. Brachet, E. Rouesne, J. Ribis, T. Guilbert, S. Urvoy, G. Nony, C. Toffolon-Masclet, M. Le Saux, N. Chaabane, H. Palancher, A. David, J. Bischoff, J. Augereau, E. Pouillier, High temperature steam oxidation of chromium-coated zirconium-based alloys: Kinetics and process, Corros. Sci. 167 (2020). doi:10.1016/j.corsci.2020.108537.